Research Article | Vol. 11, No. 6 / 1 June 2020 / Biomedical Optics Express 3288
Biomedical Optics EXPRESS

Procedure and protocols for optical imaging of cerebral blood flow and hemodynamics in awake mice

YUANDONG LI, ADIYA RAKYMZHAN, PEIJUN TANG, AND RUIKANG K. WANG*

Department of Bioengineering, University of Washington, 3720 15th Ave NE, Seattle, WA 98195, USA
**wangrk@uw.edu*

Abstract: We describe a method and procedure that allows for the optical coherence tomography angiography (OCTA) and intrinsic optical signal imaging (IOSI) of cerebral blood flow and hemodynamics in fully awake mice. We detail the procedure of chronic cranial window preparation, the use of an air-lift mobile homecage to achieve stable optical recording in the head-restrained awake mouse, and the imaging methods to achieve multiparametric hemodynamic measurements. The results show that by using a collection of OCTA algorithms, the high-resolution cerebral vasculature can be reliably mapped at a fully awake state, including flow velocity measurements in penetrating arterioles and capillary bed. Lastly, we demonstrate how the awake imaging paradigm is used to study cortical hemodynamics in the mouse barrel cortex during whisker stimulation. The method presented here will facilitate optical recording in the awake, active mice and open the door to many projects that can bridge the hemodynamics in neurovascular units to naturalistic behavior.

1. Introduction

The current generation of non-invasive optical imaging tools provide unprecedented brain access for observing and monitoring dynamics of microstructure and microcirculation in the living animal at high spatial resolution. As a result, optical imaging methods are growing in popularity in neuroscience for studying neurovascular function that pertains to local cerebral blood flow control at a microscopic level [1]. Optical coherence tomography angiography (OCTA) [2–5] is one such method, which is a label-free, depth-resolved optical imaging technique that can map three-dimensional (3D) cerebral blood perfusion to the capillary level, through analyzing the backscattering property of red blood cells (RBC) in blood stream without the use of exogenous contrast agents. Owing to the various advanced algorithms developed by several research groups, the current OCTA techniques are also available to extract quantitative perfusion parameters (e.g. velocity, flux) [6–10], enabling the study of vascular function and hemodynamics in the mouse models of stroke [11–14], aging [15], and flow-metabolism coupling [16,17]. Optical microangiography (OMAG) [18,19] has shown the ability to probe RBC velocity in the capillary bed, important for the investigation of microcirculatory pattern adjustment to cerebral tissue oxygenation during neural activity [20]. These attempts hold promise to shed new light on neurophysiological processes that underlie brain function, memory, learning, as well as injury progression and neurodegeneration.

To suppress motion artifacts during the course of high-resolution imaging, most of the optical imaging studies were carried out by immobilizing animals with general anesthesia. Although this approach is relatively simple to implement and has led to a number of exciting discoveries in the anesthetized mouse, there are many disadvantages and problems using anesthetics in the investigation of cerebral blood flow and hemodynamics. There is mounting evidence of general anesthesia influencing vascular tone [21], peripheral resistance [22], and hence cerebral blood

#394649 https://doi.org/10.1364/BOE.394649
Journal © 2020 Received 7 Apr 2020; revised 9 May 2020; accepted 19 May 2020; published 26 May 2020

Biomedical Optics EXPRESS

flow in the brain [23], which makes it difficult to precisely decipher the vascular regulation in pathological cases, such as ischemic stroke, brain trauma, and aging. Additionally, anesthetics significantly dampen the activity of neurons [24] and astrocytes [25] with altered hemodynamic coupling behavior in basal and stimulated states [26,27]. Recent studies have shown direct evidence that anesthesia lengthens the latency and time course of hemodynamic response [28,29], and that the brain activity in the rat's visual cortex in awake state cannot be reliably inferred from the findings under anesthesia [30,31]. Therefore, to enhance the neuroscientific utility of OCTA, there is a pressing need to implement the awake brain imaging paradigm in these investigations.

At present, only a limited number of approaches enable experimenting on non-anesthetized mice with two-photon microscopy [27,32], electrophysiology recording [33], or photoacoustic imaging [34,35]. One way to image inside the brain of a freely moving rodent is to attach a miniaturized head-mounted microscope. However, miniaturized devices tend to have limited optical performance and cannot be easily combined with multi-modal optical systems. Head-fixed or head-restrained preparation, on the other hand, is a popular choice that allows the animal's limb to move freely on an air-float apparatus (e.g. spherical treadmill) for stress release while enabling imaging to be performed in the spatially fixed brain [34,36–38]. This preparation typically involves an initial surgery under general anesthesia for installing a chronic cranial window to enhance optical access to deeper brain tissue, a rigid head mount used for head fixation, and the animal's gradual habituation to the head-restraining device for imaging. We found some difficulties incorporating the spherical treadmill into a more complex optical design. Because the sheer diameter of the ball (at least 200 mm for mice) renders the vertical size of the spherical treadmill large, which also requires a separate stereotaxic frame for the head fixation, such bulkiness hinders its application with a multi-modal optical system. Aside from the hardware struggle, we also acknowledged a paucity of published methods detailing the preparation of the chronic cranial window and the handling/training of the animal for head restraint.

In this paper, we introduce a simple apparatus of air-lifted flat-floor mobile homecage [39] to perform head-restrained awake mouse imaging on OCTA platforms. We delineate methods to prepare the awake mouse for optical imaging from the initial cranial window surgery to the successful awake, head-restrained imaging. We apply OMAG algorithms to perform high-resolution microangiography and velocity mapping in vessels of different calibers. Lastly, we demonstrate the application of the awake imaging paradigm to investigate cortical hemodynamics during whisker stimulation using a dual-modal optical system combining OCTA/OMAG and intrinsic optical signal imaging (IOSI).

2. Materials and methods

2.1. General experiment timeline

All experimental procedures in this study were approved by the Institutional Animal Care and Use Committee (IACUC) of the University of Washington and conducted in accordance with the ARRIVE guidelines. Three C57BL/6 mice (The Jackson Laboratory, 3-month-old, 23-28 g) was used. The mouse was pre-weighed to determine the volume of analgesics and anti-inflammatory drug, and housed individually in the cage one day before surgery. Figure 1(A) schemes the timeline of the entire experiment. On Day 0, a cranial window surgery (Section 2.2) was performed to the mouse under isoflurane general anesthesia, followed by surgical recovery for 7 days in the vivarium. No imaging and training were performed during the recovery period, except for basic post-surgical monitoring and digital photo taking of the cranial window. Starting from Day 8, the mouse was brought back to the lab every day for at least 4 continuous days of handling and training (Section 2.3) in order for it to acclimate to the laboratory environment, the experimenter, and the head-restraining device. In the first attempt of awake imaging, which usually starts on Day 12 of the study, the mouse received an additional training session right before the head-restrained imaging taken place. The maximum time required for head-restrained

Biomedical Optics EXPRESS

imaging with both IOSI and OCTA (Section 2.4 and 2.5) was 40 min. For demonstration purpose, we performed IOSI and all three OCTA protocols in the mouse, but the protocols can be selectively performed depending on the purpose of future studies. The mouse can be imaged every day if handled and trained well for up to 4 months. On the last day of the experiment, the mouse can be either anesthetized for imaging followed by euthanasia or be directly euthanized under anesthesia. The sections below detail the methods and materials used in each of the major steps.

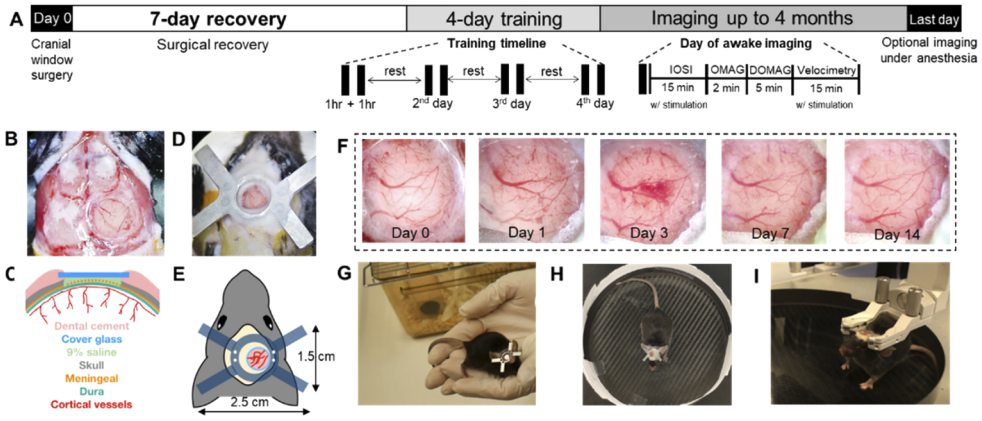

Fig. 1. A) Experimental timeline. Each animal receives a chronic cranial window and head plate installation on Day 0, followed by 7 days of recovery and at least 4 days of training. On each day of the training, the animal receives two 1-hr training sessions composed of 3 steps to acclimate to head restraining. The animal returns to the cage to rest between training sessions. On the day of awake imaging, the animal receives an additional training before being head-restrained. The maximum time required for IOSI (with whisker stimulation), OMAG, DOMAG and Velocimetry (with whisker stimulation) is 15 min, 2 min, 5 min, and 15 min, respectively. The chronic cranial window can be imaged for several months. On the last day, the animal is anesthetized again, optional imaging can be performed. B) Microscope image of a newly installed cranial window. C) Cross-sectional anatomy of the craniotomy. D) Microscope image of a newly installed head plate. E) Schematics and dimension of the cranial implants. F) Series of microscope images of the cranial window from Day 0 to Day 14. G), H), and I) The 3-step handling/training to the head-restraining device. See Visualization 1 for movie.

2.2. *Cranial window surgery and head plate installation*

The complete protocol of the chronic cranial window can be found in [40], but some modifications are needed for our study. The surgery was performed in a sterile field with aseptic techniques to minimize the risk of postoperative complications. One hour before the surgery, the mouse received buprenorphine SR (1.0 mg/kg, Zoopharm). Isoflurane (1.5-2%, Baxter) was introduced for surgical level anesthesia, which was delivered to the mouse in a mixture of 0.2 L/min pure oxygen and 0.8 L/min air through a nose cone on a stereotaxic frame with a heating pad to keep body temperature of ~36.8 °C. After the induction of anesthesia, dexamethasone sodium phosphate (2.0 mg/kg, Fresenius USA) was administered subcutaneously to reduce cortical stress and prevent cerebral edema, and the surgical site was sterilized with the alternating use of betadine and 70% alcohol. An incision was made to remove the scalp covering the cranium, and periosteum was gently retracted and scrapped to later help the dental cement adhere better to the bone. Small drops of 1% xylocaine (Lidocaine 1% + epinephrine 1:100,000 solution, Hospira) were applied to minimize bleeding of the skin and periosteum. Then, a 4-mm diameter circular

Biomedical Optics EXPRESS

craniotomy in the right parietal bone, 1 mm posterior and lateral to the bregma, was made by a dental drill with pauses 15 seconds apart for cooling with 0.9% sterile saline solution. Extra cautions were taken to prevent damage to the dural and cortical vessels, but some meningeal capillaries might tear and cause focal bleeding during removal of the cranial bone, for which case the bleeding could be stopped by applying sterile saline-soaked Gelfoam (Pfizer). When sealing cranial window with a 5-mm circular coverglass, 0.9% saline was applied as a coupling media between the glass and exposed dura, so that glue materials were not in direct contact with the brain tissue. Cyanoacrylate glue (Krazy glue) was used to seal the coverglass to the open skull. The outcome of the cranial window with cross-sectional anatomy is shown in Fig. 1(B) and Fig. 1(C). A thin layer of dental cement (Stoelting Co.) was applied to cover the rest of the skull surface, resulting in a cement head cap. Lastly, another layer of dental cement was applied on the head cap to install the metal head plate as shown in Fig. 1(D) and Fig. 1(E). After confirming that there were no exposed muscle and flesh in the surgical opening, the animal was taken off anesthesia and started the recovery process. Acute imaging under anesthesia is possible, but was not needed in this study. A lookup table for procedure and substances involved in this section can be found in Table 1.

2.3. Surgical recovery, animal handling and training

The mouse was allowed to recover from the surgery in a warmed cage with easily accessible food and water. Because Buprenorphine SR were given prior to the surgery that can provide analgesia for sustained period of 72 hours, no additional analgesics was needed unless the animal showed signs of pain and distress. A high-ceiling cage was used to prevent the animal from damaging the cranial implants. As shown in the series of camera photos in Fig. 1(F) captured during the cranial window recovery, the clarity decreased in the first 3 days with mild cerebral edema, but improved over time without drug treatment, and became stable after Day 7. Here, anti-inflammatory drugs (e.g. Carprofen) can be administered daily to further prevent complications.

To alleviate the stress of head fixation, the mouse will be able to move in an air-float Mobile HomeCage (Neurotar Oy. Ltd., Finland) freely without creating torque against the head restraint. Training was given to the animal for it to acclimate to this apparatus following three steps. 1) The mouse was habituated to the experimenting area, including the area near the head-restraining apparatus and imaging device. This includes animal handling by laboratory personnel in the imaging area by allowing free hand-to-hand movement and exploration with repeated episodes for ~15 min (Fig. 1(G)). 2) The mouse was accustomed to the floating cage by being allowed to explore within the cage without being head-restrained for ~15 min (Fig. 1(H)). 3) The mouse was acclimated to head fixation initially with short duration of head held manually by the experimenter starting at 1~2 sec and gradually increasing in time, followed by brief attachment to the head restraint holder for 1~2 min (Fig. 1(I)). This process of the gradual head restraining was repeated with a lengthening period of restraint until the mouse was fully acclimated, an example which was recorded in Visualization 1. The duration of one 3-step training session lasted ~1 hr, and two training sessions were performed in one day. A minimal 4-day training was performed before optical imaging.

2.4. System setup

An in-house built dual-modality optical imaging platform [41] was used as shown in Fig. 2(A). The spectral-domain OCT (SD-OCT) system was equipped with a broadband superluminescent diode (SLD) light source (LS2000B, Thorlabs Inc.) of 1310 ± 110 nm, yielding an axial resolution of ~5.1 μm in mouse brain tissue. The incoming light was divided into two paths through a 2×2 optical coupler to reference arm and sample arm. In the sample arm, the light passed through a custom-designed unit containing a collimator, a paired x-y galvanometer (6200H, Novanta/Cambridge Technology) and a 10× objective lens (LSM02, Thorlabs Inc.) with a

Biomedical Optics EXPRESS

Table 1. Procedure and substance lookup table for the chronic cranial window surgery

Step	Procedure description	Materials & substance	Remarks
1	One hour prior to surgery, administer buprenorphine SR subcutaneously. Prepare sterile supplies and instruments.	• Buprenorphine-sustained release (SR) (ZooPharm, 0.5 mg/ml). Dosage: 1.0 mg/kg.	Buprenorphine SR can provide analgesia for sustained period of 72 hours. Alternatively, standard buprenorphine (0.05 mg/kg) can be used here and then 8-12 hours after the surgery for 3 days.
2	Induce anesthesia to the animal by isoflurane inhalation in oxygen enriched air (0.2 L/min O_2 and 0.8 L/min air), firstly at 5% dose in an induction chamber, and then adjust to 1.5-2% after transferring the animal to the nose cone on the stereotaxic frame.	• Isoflurane (FORANE, Baxter, USA). Dosage: 5% initially, and then 1.5~2% throughout the surgery.	
3	Administer dexamethasone subcutaneously, and mount the mouse head using an ear bar adapter. Apply eye ointment to prevent the cornea from drying out.	• Dexamethasone sodium phosphate injection (Fresenius USA, 4 mg/ml). Dose: 2.0 mg/kg • Refresh P.M. Lubricant Eye Ointment	Dexamethasone reduces the cortical stress response and prevents cerebral edema. It is critical for successful surgeries.
4	Remove the scalp hair by Nair cream. Sterilize the surgical site by alternating betadine and 70% alcohol at least three times. Drape the animal and set up a sterile field.	• Nair™ hair lotion • Betadine surgical scrub (Avrio Health LP) • 70% isopropanol (Fisher Co., USA)	Going to a sterile field after this step.
5	Make an incision to remove the scalp covering the cranium, gently retract the skin and scrap off the periosteum. Use small drops of 1% xylocaine to minimize bleeding of the skin and periosteum tissue.	Xylocaine liquid (lidocaine 1% + epinephrine 1:100,000 solution, Hospira, USA)	Removing the periosteum tissue will later help the dental cement adhere to the bone and better secure the cranial implant.
6	Use a dental drill with a round carbide bur to create circular groove in the right parietal bone, 1 mm posterior and lateral to the bregma. Pause drilling every 15 sec to apply 0.9% sterile saline to avoid heating. Leave the central island of skull (dia. 4-mm) intact.	• High-speed surgical hand drill (Foredom, USA) with #2 round FG carbide burs (0.5 mm). • Sterile saline 0.9% (Mountainside Medical, USA)	Extra cautions should be taken not to apply excessive pressure with the drill that may puncture the skull and injure the dura. Check the readiness of the craniotomy by gently pushing on the center island with forceps. If the island moves when lightly touched, then it is ready to be lifted/removed.
7	Apply saline drops, then gently insert the tip of an angled-fine-tipped forceps into the trabecular (spongy) bone of the center island, horizontally, from the side of the groove, and slowly lift/remove the center island. If bleeding occurs, use saline-soaked Gelfoam to clean up the blood or keep the exposed dura moist.	• Sterile Gelfoam sponges (Pfizer, USA)	Saline is important here to help with lifting the center island and have it removed without excessive bleeding. Some meningeal capillaries might tear and cause focal bleeding during the removal. Use only Gelfoam to soak up the blood and clean the exposed dura, cotton swabs or Kimwipes are discouraged.
8	Replace the center island of skull with a 5-mm circular coverglass, apply a drop of saline as a coupling media in between, and then use cyanoacrylate glue to seal the coverglass.	• Krazyglue (Krazy Glue, USA)	It is important to use saline here as a coupling media between the glass and dura, so that glue materials were not in direct contact with brain tissue.
9	Apply a thin layer of dental cement to cover the rest of the skull surface, resulting in a cement headcap. After drying this layer, apply another layer of cement to install the medal plate.	• Dental cement (Stoelting Co., USA)	Check to make sure all areas are covered with dental cement with no exposed muscle and flesh in the surgical opening.

Biomedical Optics EXPRESS

working distance of 18 mm, providing ~10 μm lateral resolution. The light backscattered from the sample was combined with the one reflected from the reference mirror and transmitted to a home-built spectrometer with a spectral resolution of 0.141 nm, providing an imaging depth of 2.22 mm into the sample. A high speed InGaAs line-scan camera (SUI, Goodrich Corp.) was used in the spectrometer to capture the interferograms at a best recording speed of 92,000 A-line/sec.

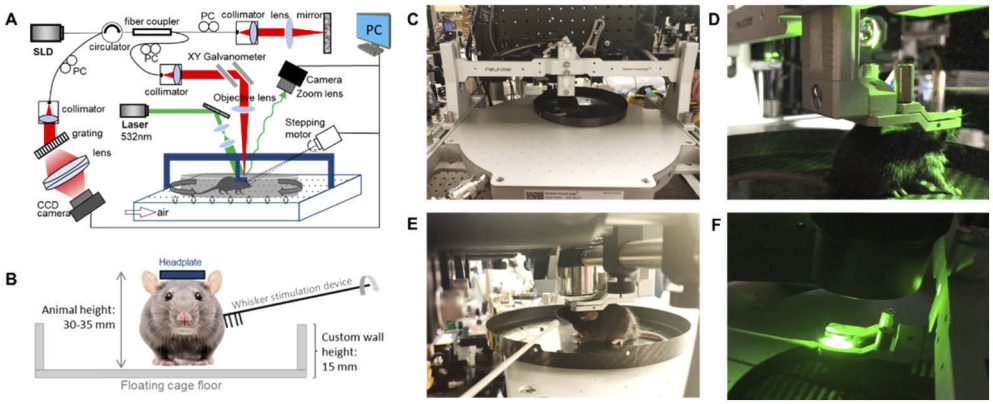

Fig. 2. A) Schematic diagram of the optical imaging system. SLD: superluminescent diode, PC: polarization controller, PC (bold): personal computer. B) Schematic diagram of the mouse whisker stimulation setup. C) and E) Imaging with OCT. D) and F) Imaging with IOSI. See Visualization 2 for movie.

Right next to the SD-OCT was a simple setup for intrinsic optical signal imaging (IOSI). It contained a single-mode laser diode with a wavelength of 532 nm (MGL-III-532, CNI Optoelectronics Technology Co. Ltd.) illuminating the sample at 30° angle from the tissue surface. The diffusely reflected light from the tissue was detected with a CMOS camera (A504k 1280×1024 pixels, Basler) through a zoom lens with provided adjustable magnification.

The animal was head-restrained, but allowed to walk, run, or rest still on the air-float homecage while imaging is performed on OCT and IOSI platform (Fig. 2(C) and (D)). We also implemented a custom carbon cage with a wall height of 15 mm, shown in Fig. 2(B), which allowed for the access of whisker stimulation devices. We used a cotton applicator-connected stepping motor synchronized imaging acquisition to perform whisker stimulations (Fig. 2(E) and (F)). Demonstration of the optical imaging in the head-restrained awake mouse is found in Visualization 2.

2.5. *Imaging protocols and algorithms*

Optical microangiography (OMAG) [19] was used to achieve high-resolution mapping of the cerebral vasculature. In this protocol, the B-scan consisted of 400 A-lines was repeated 8 times at each transverse location to extract blood flow information with the OMAG algorithm. A total of 400 blood flow B-frames was acquired. The *en face* projection of the 3D volume covered a 4 × 4 mm region in the cranial window. The data was acquired with A-line rate of 72 kHz and B-scan rate of 180 fps, requiring an acquisition time of ~15 sec.

Doppler OMAG (DOMAG) [7] was applied to map the axial velocity of cerebral penetrating vessels. This protocol was performed with 25 A-lines repeatedly acquired at each depth location for axial velocity calculation from phase Doppler principle, and 300 locations were recorded in one B-frame. A total of 300 B-frames was captured to accomplish a 3D dataset. The total scanning time of each dataset was ~50 sec at A-line rate of 45 kHz and B-frame rate of 6 fps.

Biomedical Optics EXPRESS

Each 3D dataset covered a 2.5 × 2.5 mm region, and 4 quadrants of data were taken and montaged together to cover the entire region of the craniotomy.

A recently developed capillary velocimetry based on OMAG was applied to measure flow velocities in the capillary bed [18]. In this protocol, the A-line rate were set to be 20 kHz with 50 repetition performed at each depth location. This setting yielded adjustable calculated A-line interval from 50 μm to 2.5 ms to potentially capture slow to fast capillary flows from 100 μm/s to 5 mm/s. An eigendecomposition (ED) analysis was applied to the 50-scan ensemble to extract the frequency components of the single-file moving RBC in capillary passages. Each B-frame consisted of 100 locations, a total number of 100 B-frames were acquired in one 3D dataset. Each velocimetry map covered an 800×800 μm region, taking ~30 sec to complete one data acquisition.

For IOSI, magnification was set with 2.5 with an imaging field of view of ~5.5×5.5 mm^2, which makes the speckle size roughly twice of the size of the camera pixels to maximize the contrast of the speckle patterns [41]. The camera exposure was 40 ms and the sampling rate was 15 Hz. For each data set, 600 frames were captured for 40 sec recording in the mouse brain, during which period whisker stimulation was applied from 10 to 20 sec. After finishing recording the raw reflectance images, the first 10 frames were averaged and used as a baseline. This baseline was subtracted by each of the following frames and the resulting image were normalized to baseline. Then, the time-lapse full field transversal 2D images representing the relative changes in reflectance were obtained.

2.6. Whisker stimulation

Whisker stimulations were performed to demonstrate the recording of hemodynamic changes in the awake mouse with IOSI and OCTA velocimetry. Whiskers of the contralateral side to the craniotomy were contacted circularly by a cotton application, connected to a 2-phase stepping motor rotate at 3 Hz during the stimulation. During IOSI, within the 40 secs of data acquisition, whisker stimulation was applied between 10 ~ 20 sec. Guided from the relative reflectance maps, barrel cortex (R1) and a control area (R2) were identified, where OCTA capillary velocimetry scans were targeted during 30 sec of rest and 30 sec of whisker stimulation, respectively.

2.7. Data analysis

All optical images were produced in Matlab (Mathworks, MA, USA) using in-house developed codes. The image segmentation software is written in Python.

3. Results

3.1. Cerebral blood flow imaging in the awake mouse with OMAG

High resolution vasculature maps and blood perfusion dynamics were obtained with OMAG in the awake mouse at Day 14 shown in Fig. 3. All results in this figure were obtained in the awake mouse during the resting state (no stimulation). Figure 3(A) shows the *en face* projection of the 3D vasculature. The cross sections of OCT structure in Fig. 3(B) and OMAG blood flow in Fig. 3(C) have indicated a thin layer of vessel-enriched meningeal tissue growing above the cortical layer that are not found in acute cranial windows [42]. To enhance the visualization of cortical vasculature, we used a semi-automatic segmentation software [43] to separate the meningeal layer (L1) and cortical layer (L2) as indicated by the yellow segmentation line in Fig. 3(C). After removing the tailing artifact [44] from L1 and flattening each layer, new *en face* projection images are made and shown to the right. Here, cortical vasculature in L2 can be better contrasted as compared to the original project image in Fig. 3(A).

Figure 3(D) shows the *en face* projection the bi-directional axial velocity of penetrating arterioles (green) and rising venules (red) with velocity range from 6.1 mm/s to -6.1 mm/s. Some

Biomedical Optics EXPRESS

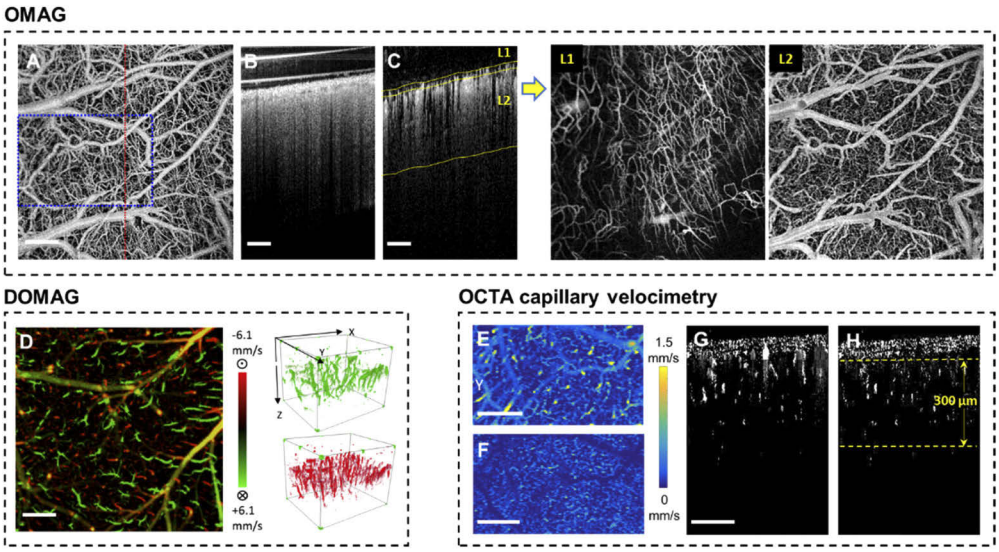

Fig. 3. A) *En face* maximum intensity projection (MIP) of the full-depth 3D OMAG dataset acquired in the awake mouse during resting state on Day 14 after the cranial window surgery. B) Cross section of the OCT structure in the red-dashed line position in A. (C) Cross section of the OMAG blood flow with yellow segmentation line for L1 and L2. The new *en face* images of the two segmented layers are shown to the right. D) Bi-directional axial velocity map generated by *en face* MIP of the 3D DOMAG dataset. Color bar represents RBC axial velocity of the flow descending (positive, green) and rising from (negative, red) the cortical surface in a range of ±6.1 mm/s. The 3-D velocity signals are shown to the right of the projection image. E) and F) are showing the *en face* average intensity projection (AIP) of the 3D capillary velocimetry dataset within 300 μm thickness slab with and without masking, corresponding to their cross sections in G and H, respectively. All scale bars in this figure represent 500 μm.

yellow colored vessels are appeared due to a mix of green and red signals from the projection effect. The arteriole and venules signals in the 3D space are shown to the right.

Figure 3(E) shows the *en face* projection of capillary velocity obtained from the measured cortical volume. For more accurate evaluation of capillary dynamics, masking was applied to remove signals in larger vessels with a diameter larger than 15 μm. The further processed velocity map is shown in Fig. 3(F). Cross sections in Fig. 3(G) and Fig. 3(H) demonstrate the difference before and after masking large flow signals. In the dataset shown, >20,000 velocity signals were obtained within the 300-μm thickness slab as indicated in Fig. 3(H).

3.2. Hemodynamics of whisker stimulation in the awake mouse

Neuroactivity-induced hemodynamic changes at the mouse barrel cortex at awake state is revealed by IOSI in Fig. 4(A). The top map shows the relative reflectance (-ΔR/R) at 2 sec of image capturing when whisker stimulation has not yet applied. The bottom map shows the -ΔR/R map at 15 sec of image acquisition (with 5 sec of whisker stimulation). Here, the hemodynamic response evoked by stimulation is observed as higher contrast in the blood vessel against the background parenchyma, corresponding to a local increase in total hemoglobin (hyperemia) in the barrel cortex due to activation. Guided by the IOSI results, OCTA capillary velocimetry scans were performed in the barrel cortex (R1) and a control region (R2). Figure 4(B)-(E) show the capillary velocity maps in these 2 regions at different states. Histogram distributions of the velocity signals are plotted to compare the differences from rest and stimulation. In R1, shown

Biomedical Optics EXPRESS

in Fig. (D), RBC velocities are statistically increased, making the distribution of stimulation state slightly skewed right. This is also in line with the observation in Fig. 4(C), where some of the velocity signals are enhanced during whisker stimulation. On the contrary, two distributions in the control region are mostly overlapped (Fig. (G)), no distribution shifts are observed upon stimulation.

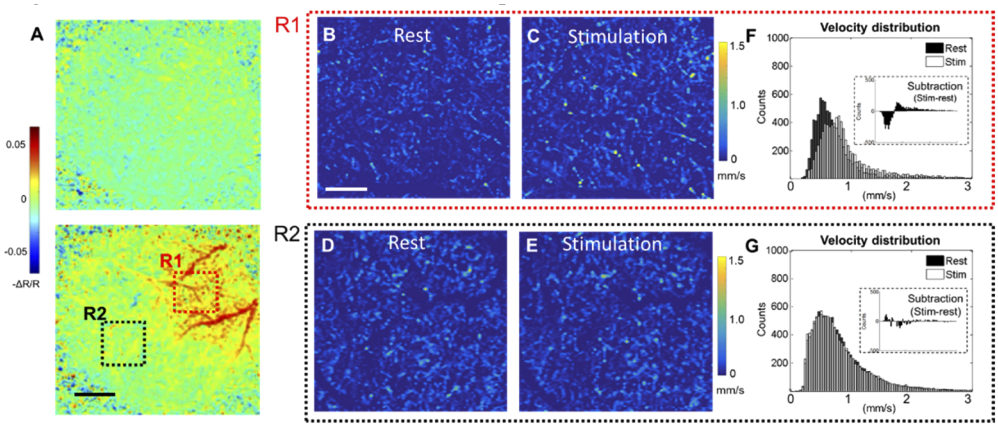

Fig. 4. A) Wide-field reflectance mapping of the mouse barrel cortex during whisker stimulation achieved with IOSI. Top: 2 sec of data acquisition (no stimulation). Bottom: 15 sec of data acquisition (5 sec of whisker stimulation). R1 indicate an activation of hemodynamic response during whisker stimulation, and R2 is a control region with no response observed. Scale bar represents 1 mm. B)-E) are *en face* AIP images of the 3D velocimetry dataset at two regions during different states. Images are produced within 300 μm thickness slab after masking out large vessels, the remaining capillary velocity signals are plotted with histogram distributions for F (R1) and G (R2). Insets in the distribution histogram indicate the subtraction from stimulation to rest. Scale bar for velocimetry maps represents 200 μm.

4. Discussion

Imaging of awake animals is necessary to fully understood neurovascular coupling during naturalistic sensorimotor activity, but experiments on awake and behaving mice have represent a significant methodological challenges. To our best knowledge, there has been no publications detailing the methods and protocols to achieve cerebral blood flow and hemodynamic imaging in awake mouse using optical imaging approach. In this paper, we have provided instructions that include a description of surgical techniques to obtain optical access to the cortex, training and acclimation protocols to adapt the animal to an improved head-restraint device, and robust imaging algorithms to resolve cerebral vasculature and measure blood flow velocity at the level of single cortical vessels.

The use of air-lifted homecage was introduced for the first time to OCTA imaging. This apparatus ensures the mechanical stability of the brain while allowing the mouse to explore its tangible environment under stress-free conditions. A variety of OCTA algorithms, including OMAG, DOMAG, and capillary velocimetry, were achieved in the mouse brain in awake state with uncompromised quality (Fig. 3) as compared to the anesthetic imaging [15], and no obvious motion artifacts were observed. Visualization 3 shows a 2D OCT structure B-scan movie of 400 frames acquired over 10 seconds to demonstrate the stability of the cranial window when the mouse was fully awake and walking in the homecage while being head-restrained. The worst correlation coefficient between the first B-scan and rest of B-scans in the entire duration of

Biomedical Optics EXPRESS

the movie (10 sec) was 0.93. Additionally, IOSI and OCTA capillary velocimetry were both accomplished to reveal changes in HbT and capillary flow velocity distribution, respectively, during whisker stimulation in the mouse barrel cortex (Fig. 4). Aside from this demonstration, the device should be readily applicable to other types of stimulation (e.g. visual) using a range of optical imaging modalities. The compact design of the mobile homecage will allow positioning under most standard upright microscope objectives for imaging and recording in the awake mouse brain.

Maintenance of the chronic cranial window quality is one of the determining factors of optical image quality. The surgical procedure in this study was developed based on years of experience adapting from previously published protocols, and was found to result in a stable and reproducible cranial window preparation for longitudinal studies that last for several months. During the surgical recovery, the window first transiently loses its transparency and then regains it after about a week. Cerebral edema is occasionally observed during this period, but can be self-absorbed over time in most cases (Fig. 1(F)). In our experiences, the cranial window clarity usually returns with about 70% yield at around Day 7 and remains stable thereafter, but more time (2-3 weeks) should be given if there are any signs of inflammation or internal bleeding, for which case anti-inflammatory drugs (e.g. carprofen) can be administered daily to facilitate the clearance.

It should be noted that during the surgical procedure, meningeal capillaries on the dura surface often will tear when detaching the cranium from dura, shown as the orange dashed line inside craniotomy in Fig. 1(C). These vessels gradually repair inside the sealed cranial window and then reform a thin layer of meningeal vessel network on the cortical surface. While this vessel regrowth is not visible in the microscope images, and may not interfere with neuroimaging of cellular or molecular structure, the sensitive OMAG detection has picked up the blood flow in this layer, which create problems when quantifying cortical vascular features, such as capillary density, flux, from the *en face* image (Fig. 3(A)). Segmentation has effectively solved this problem by extracting the meningeal vessels (L1 in Fig. 3(C)) and eliminate it to create better visualization of the cortical blood vessel network.

Since acutely performed awake experiments are typically untenable when the animal is naïve to the imaging apparatus, proper training needs to be provided after the animal recovers from the surgery. We have outlined a sample training protocol in Section 2.3, but the time and sessions required for fully acclimate to the imaging paradigm will vary among individual mice, thus the pace of training should be adjusted. The goal is to have the mouse freely ambulating on the homecage. Administration of tranquilizer was not needed in this experiment, but can be administered to reduce the anxiety of the animal when prolonged imaging time (>1hr) is necessary in the study design. Training the mouse is a critical step for functional studies in awake, behaving animals, not only for cortical stress release, but also for generating a relatively stable sensorimotor baseline to obtain proper somatosensory signal upon external stimulation. When an animal is first exposed to a new environment, its behavior would be exploratory and anxious, which would induce sensorimotor responses, leading to a crosstalk between movement and sensation due to the natural sensorimotor integration of the nervous system. During the training and habituation, it has been reported that an efferent copy of the sensorimotor system would enable the brain to adaptively estimate the sensory feedback from movements within the tangible environment [45], where a new baseline is eventually established. Thereafter, the animal would be able to accept additional commands on top of the baseline. As the mouse moved calmly and spontaneously in the head-restrained device, the activation map observed in our study is considered due to stimulus-induced (e.g. whisker tapping) somatosensory activation.

The custom-built dual-modal optical platform (Fig. 2) is a great tool to investigate the meso-to-micro-scale level cerebra blood flow and hemodynamics. The high-resolution angiograms produced by OMAG (Fig. 3(A)-(C)) enables quantitative analyses of vasculature features, including, but not limited to, arteriole diameter, tortuosity, and capillary density [15]. From

Biomedical Optics EXPRESS

the axial velocity maps generated with DOMAG (Fig. 3(D)), cross-sectional flow area of the penetrating vessels can be calculated as well as the total blood flow. From the capillary velocimetry mapping (Fig. 3(F)), additional parameters, such as mean transit time and capillary transit time heterogeneity, may be deduced to decipher the microvascular flow pattern. In the demonstration of whisker stimulation study, IOSI provides wide-field optical mapping to facilitate the identification of functional cortex, which guides OCTA capillary velocimetry to be performed efficiently in smaller region of interest in barrel cortex. The results in Fig. 4 indicates that in activated region, R1, the mean capillary velocity increased, which is in agreement with functional hyperemia observed by IOSI. The pattern of changes is also consistent with the one obtained from anesthetized mice [20]. Further experiments and analysis are warranted to gain more statistics in the awake animal.

Lastly, aside from the investigation of neurovascular function, the awake mouse imaging can be also applied in longitudinal study with a variety of purposes when multiple imaging sessions are needed. Time intervals between repeated imaging/recording are more flexible since no additional anesthesia and lengthy recovery is needed. Many potential projects are anticipated, including the longitudinal study of vascular changes in brain aging and neurodegenerative diseases.

5. Conclusion

In summary, we have presented a protocol and experimental method to perform OCTA and ISOI in fully awake mouse. The use of the air-lifted mobile homecage greatly facilitates the head-restraint during awake imaging, and high-quality OCTA/OMAG imaging can be achieved in the brain of animal in fully awake state. The setup also works well with external stimulation models for the investigation of functional neurovascular activity with OCTA and IOSI. The methods and protocols presented in this paper are instructional for optical imaging of cerebral blood flow in the awake mouse, which is expected to open new horizons in experimentation on awake behaving animals for the basic research of brain functions and drug developments.

Funding

National Heart, Lung, and Blood Institute (R01 HL093140); Washington Research Foundation; Research to Prevent Blindness.

Disclosures

None.

References

1. E. M. C. Hillman, "Optical brain imaging in vivo: techniques and applications from animal to man," J. Biomed. Opt. **12**(5), 051402 (2007).
2. C.-L. Chen and R. K. Wang, "Optical coherence tomography based angiography [Invited]," Biomed. Opt. Express **8**(2), 1056–1082 (2017).
3. T. E. de Carlo, A. Romano, N. K. Waheed, and J. S. Duker, "A review of optical coherence tomography angiography (OCTA)," Int. J. Retin Vitr. **1**(1), 5 (2015).
4. A. H. Kashani, C.-L. Chen, J. K. Gahm, F. Zheng, G. M. Richter, P. J. Rosenfeld, Y. Shi, and R. K. Wang, "Optical Coherence Tomography Angiography: A Comprehensive Review of Current Methods and Clinical Applications," Prog. Retinal Eye Res. **60**, 66–100 (2017).
5. S. S. Gao, Y. Jia, M. Zhang, J. P. Su, G. Liu, T. S. Hwang, S. T. Bailey, and D. Huang, "Optical Coherence Tomography Angiography," Invest. Ophthalmol. Visual Sci. **57**(9), OCT27–36 (2016).
6. J. Lee, W. Wu, F. Lesage, and D. A. Boas, "Multiple-Capillary Measurement of RBC Speed, Flux, and Density with Optical Coherence Tomography," J. Cereb. Blood Flow Metab. **33**(11), 1707–1710 (2013).
7. L. Shi, J. Qin, R. Reif, and R. K. Wang, "Wide velocity range Doppler optical microangiography using optimized step-scanning protocol with phase variance mask," J. Biomed. Opt. **18**(10), 106015 (2013).
8. V. J. Srinivasan, H. Radharishnan, E. H. Lo, E. T. Mandeville, J. Y. Jiang, S. Barry, and A. E. Cable, "OCT methods for capillary velocimetry," Biomed. Opt. Express **3**(3), 612–629 (2012).

Biomedical Optics EXPRESS

9. W. J. Choi, W. Qin, C.-L. Chen, J. Wang, Q. Zhang, X. Yang, B. Z. Gao, and R. K. Wang, "Characterizing relationship between optical microangiography signals and capillary flow using microfluidic channels," Biomed. Opt. Express **7**(7), 2709–2728 (2016).
10. J. Tang, S. E. Erdener, B. Fu, and D. A. Boas, "Capillary red blood cell velocimetry by phase-resolved optical coherence tomography," Opt. Lett. **42**(19), 3976–3979 (2017).
11. V. J. Srinivasan, E. T. Mandeville, A. Can, F. Blasi, M. Climov, A. Daneshmand, J. H. Lee, E. Yu, H. Radhakrishnan, E. H. Lo, S. Sakadžić, K. Eikermann-Haerter, and C. Ayata, "Multiparametric, Longitudinal Optical Coherence Tomography Imaging Reveals Acute Injury and Chronic Recovery in Experimental Ischemic Stroke," PLoS One **8**(8), e71478 (2013).
12. W. J. Choi, Y. Li, and R. K. Wang, "Monitoring acute stroke progression: multi-parametric OCT imaging of cortical perfusion, flow, and tissue scattering in a mouse model of permanent focal ischemic," IEEE Trans. Med. Imag. **38**(6), 1427–1437 (2019).
13. J. Lee, Y. Gursoy-Ozdemir, B. Fu, D. A. Boas, and T. Dalkara, "Optical coherence tomography imaging of capillary reperfusion after ischemic stroke," Appl. Opt. **55**(33), 9526–9531 (2016).
14. Y. Nishijima, Y. Akamatsu, S. Y. Yang, C. C. Lee, U. Baran, S. Song, R. K. Wang, T. Tominaga, and J. Liu, "Impaired Collateral Flow Compensation During Chronic Cerebral Hypoperfusion in the Type 2 Diabetic Mice," Stroke **47**(12), 3014–3021 (2016).
15. Y. Li, W. J. Choi, W. Wei, S. Song, Q. Zhang, J. Liu, and R. K. Wang, "Aging-associated changes in cerebral vasculature and blood flow as determined by quantitative optical coherence tomography angiography," Neurobiol. Aging **70**, 148–159 (2018).
16. E. Gutiérrez-Jiménez, C. Cai, I. K. Mikkelsen, P. M. Rasmussen, H. Angleys, M. Merrild, K. Mouridsen, S. N. Jespersen, J. Lee, N. K. Iversen, S. Sakadzic, and L. Østergaard, "Effect of electrical forepaw stimulation on capillary transit-time heterogeneity (CTH)," J. Cereb. Blood Flow Metab. **36**(12), 2072–2086 (2016).
17. J. Lee, W. Wu, and D. A. Boas, "Early capillary flux homogenization in response to neural activation," J. Cereb. Blood Flow Metab. **36**(2), 375–380 (2016).
18. R. K. Wang, Q. Zhang, Y. Li, and S. Song, "Optical coherence tomography angiography-based capillary velocimetry," J. Biomed. Opt. **22**(6), 066008 (2017).
19. R. K. Wang, S. L. Jacques, Z. Ma, S. Hurst, S. R. Hanson, and A. Gruber, "Three dimensional optical angiography," Opt. Express **15**(7), 4083–4097 (2007).
20. Y. Li, W. Wei, and R. K. Wang, "Capillary flow homogenization during functional activation revealed by optical coherence tomography angiography based capillary velocimetry," Sci. Rep. **8**(1), 4107 (2018).
21. K. Engelhard and C. Werner, "The effects of general anesthesia and variations in hemodynamics on cerebral perfusion," Applied Cardiopulmonary Pathophysiology **13**, 157–159 (2009).
22. T. Akata, "General Anesthetics and Vascular Smooth MuscleDirect Actions of General Anesthetics on Cellular Mechanisms Regulating Vascular Tone," Anesthesiology **106**(2), 365–391 (2007).
23. A. M. Slupe and J. R. Kirsch, "Effects of anesthesia on cerebral blood flow, metabolism, and neuroprotection," J. Cereb. Blood Flow Metab. **38**(12), 2192–2208 (2018).
24. N. P. Franks, "General anaesthesia: from molecular targets to neuronal pathways of sleep and arousal," Nat. Rev. Neurosci. **9**(5), 370–386 (2008).
25. A. S. Thrane, T. V. Rangroo, D. Zeppenfeld, N. Lou, Q. Xu, E. A. Nagelhus, and M. Nedergaard, "General anesthesia selectively disrupts astrocyte calcium signaling in the awake mouse cortex," Proc. Natl. Acad. Sci. U. S. A. **109**(46), 18974–18979 (2012).
26. P. J. Drew, A. Y. Shih, and D. Kleinfeld, "Fluctuating and sensory-induced vasodynamics in rodent cortex extend arteriole capacity," Proc. Natl. Acad. Sci. U. S. A. **108**(20), 8473–8478 (2011).
27. A. Y. Shih, P. J. Drew, and D. Kleinfeld, "Imaging Vasodynamics in the Awake Mouse Brain with Two-Photon Microscopy," *Neurovascular Coupling Methods. Neuromethods*, 88. Humana Press, New York, NY (2014).
28. C. Martin, J. Martindale, J. Berwick, and J. Mayhew, "Investigating neural-hemodynamic coupling and the hemodynamic response function in the awake rat," NeuroImage **32**(1), 33–48 (2006).
29. K. Masamoto, M. Fukuda, A. Vazquez, and S.-G. Kim, "Dose-dependent effect of isoflurane on neurovascular coupling in rat cerebral cortex," Eur. J. Neurosci. **30**(2), 242–250 (2009).
30. M. A. Pisauro, N. T. Dhruv, M. Carandini, and A. Benucci, "Fast hemodynamic responses in the visual cortex of the awake mouse," J. Neurosci. **33**(46), 18343–18351 (2013).
31. D. S. Greenberg, A. R. Houweling, and J. N. D. Kerr, "Population imaging of ongoing neuronal activity in the visual cortex of awake rats," Nat. Neurosci. **11**(7), 749–751 (2008).
32. M. Desjardins, K. Kılıç, M. Thunemann, C. Mateo, D. Holland, C. G. L. Ferri, J. A. Cremonesi, B. Li, Q. Cheng, K. L. Weldy, P. A. Saisan, D. Kleinfeld, T. Komiyama, T. T. Liu, R. Bussell, E. C. Wong, M. Scadeng, A. K. Dunn, D. A. Boas, S. Sakadžić, J. B. Mandeville, R. B. Buxton, A. M. Dale, and A. Devor, "Awake Mouse Imaging: From Two-Photon Microscopy to Blood Oxygen Level-Dependent Functional Magnetic Resonance Imaging," Biol. Psychiatry Cogn. Neurosci. Neuroimaging. **4**(6), 533–542 (2019).
33. M. S. Fee, "Active stabilization of electrodes for intracellular recording in awake behaving animals," Neuron **27**(3), 461–468 (2000).
34. R. Cao, J. Li, B. Ning, N. Sun, T. Wang, Z. Zuo, and S. Hu, "Functional and oxygen-metabolic photoacoustic microscopy of the awake mouse brain," NeuroImage **150**, 77–87 (2017).

Biomedical Optics EXPRESS

35. J. Tang, J. E. Coleman, X. Dai, and H. Jiang, "Wearable 3-D Photoacoustic Tomography for Functional Brain Imaging in Behaving Rats," Sci. Rep. **6**(1), 25470 (2016).
36. P. S. Sharp, K. Shaw, L. Boorman, S. Harris, A. J. Kennerley, M. Azzouz, and J. Berwick, "Comparison of stimulus-evoked cerebral hemodynamics in the awake mouse and under a novel anesthetic regime," Sci. Rep. **5**(1), 12621 (2015).
37. D. A. Dombeck, A. N. Khabbaz, F. Collman, T. L. Adelman, and D. W. Tank, "Imaging Large-Scale Neural Activity with Cellular Resolution in Awake, Mobile Mice," Neuron **56**(1), 43–57 (2007).
38. C. H. T. Tran and G. R. Gordon, "Acute two-photon imaging of the neurovascular unit in the cortex of active mice," Front. Cell. Neurosci. **9**, 11 (2015).
39. M. Kislin, E. Mugantseva, D. Molotkov, N. Kulesskaya, S. Khirug, I. Kirilkin, E. Pryazhnikov, J. Kolikova, D. Toptunov, M. Yuryev, R. Giniatullin, V. Voikar, C. Rivera, H. Rauvala, and L. Khiroug, "Flat-floored air-lifted platform: a new method for combining behavior with microscopy or electrophysiology on awake freely moving rodents," J. Visualized Exp. **88**(88), e51869 (2014).
40. A. Holtmaat, T. Bonhoeffer, D. K. Chow, J. Chuckowree, V. De Paola, S. B. Hofer, M. Hübener, T. Keck, G. Knott, W. C. Lee, R. Mostany, T. D. Mrsic-Flogel, E. Nedivi, C. Portera-Cailliau, K. Svoboda, J. T. Trachtenberg, and L. Wilbrecht, "Long-term, high-resolution imaging in the mouse neocortex through a chronic cranial window," Nat. Protoc. **4**(8), 1128–1144 (2009).
41. P. Tang, Y. Li, A. Rakymzhan, Z. Xie, and R. K. Wang, "Measurement and visualization of stimulus-evoked tissue dynamics in mouse barrel cortex using phase-sensitive optical coherence tomography," Biomed. Opt. Express **11**(2), 699–710 (2020).
42. Y. Li, U. Baran, and R. K. Wang, "Application of Thinned-Skull Cranial Window to Mouse Cerebral Blood Flow Imaging Using Optical Microangiography," PLoS One **9**(11), e113658 (2014).
43. X. Yin, J. R. Chao, and R. K. Wang, "User-guided segmentation for volumetric retinal optical coherence tomography images," J. Biomed. Opt. **19**(8), 086020 (2014).
44. Q. Zhang, A. Zhang, C. S. Lee, A. Y. Lee, K. A. Rezaei, L. Roisman, A. Miller, F. Zheng, G. Gregori, M. K. Durbin, L. An, P. F. Stetson, P. J. Rosenfeld, and R. K. Wang, "Projection artifact removal improves visualization and quantitation of macular neovascularization imaged by optical coherence tomography angiography," Ophthalmol. Retina. **1**(2), 124–136 (2017).
45. M. Flanders, "What is the biological basis of sensorimotor integration?" Biol. Cybern. **104**(1-2), 1–8 (2011).